Controlled evolution of three-dimensional magnetic states in strongly coupled cylindrical nanowire pairs

OPEN ACCESS
IOP Publishing
Nanotechnology

Nanotechnology **34** (2023) 125301 (11pp) https://doi.org/10.1088/1361-6528/aca9d6

Controlled evolution of three-dimensional magnetic states in strongly coupled cylindrical nanowire pairs

J Fullerton[1,*], A Hierro-Rodriguez[2], C Donnelly[3], D Sanz-Hernández[4], L Skoric[5], D A MacLaren[1] and A Fernández-Pacheco[1,6,*]

[1] SUPA, School of Physics and Astronomy, University of Glasgow, Glasgow, United Kingdom
[2] Depto. Fisica, Universidad de Oviedo, Oviedo, Spain
[3] Max Planck Institute for Chemical Physics of Solids, Dresden, Germany
[4] Unité Mixte de Physique, CNRS, Thales, Université Paris-Saclay, Paris, France
[5] Cavendish Laboratory, University of Cambridge, Cambridge, United Kingdom
[6] Instituto de Nanociencia y Materiales de Aragón, CSIC-Universidad de Zaragoza, Zaragoza, Spain

E-mail: j.fullerton.1@research.gla.ac.uk and amaliofp@unizar.es

Received 12 October 2022, revised 2 December 2022
Accepted for publication 7 December 2022
Published 13 January 2023

Abstract

Cylindrical magnetic nanowires are promising systems for the development of three-dimensional spintronic devices. Here, we simulate the evolution of magnetic states during fabrication of strongly-coupled cylindrical nanowires with varying degrees of overlap. By varying the separation between wires, the relative strength of exchange and magnetostatic coupling can be tuned. Hence, we observe the formation of six fundamental states as a function of both inter-wire separation and wire height. In particular, two complex three-dimensional magnetic states, a 3D Landau Pattern and a Helical domain wall, are observed to emerge for intermediate overlap. These two emergent states show complex spin configurations, including a modulated domain wall with both Néel and Bloch character. The competition of magnetic interactions and the parallel growth scheme we follow (growing both wires at the same time) favours the formation of these anti-parallel metastable states. This works shows how the engineering of strongly coupled 3D nanostructures with competing interactions can be used to create complex spin textures.

Supplementary material for this article is available online

Keywords: micromagnetics, three-dimensional, coupled nanowire, focused electron beam induced deposition

(Some figures may appear in colour only in the online journal)

1. Introduction

Magnetic nanowires have been widely studied due to their great potential for technologies including data storage, logic components and biological sensing [1–6]. Moreover, it has been shown that strong coupling between multiple nanowires can lead to novel emergent behaviours. For example, ultra-fast domain wall motion can be observed in synthetic anti-ferromagnetic nanowire systems [7] and coupled nanowire rings show promise for reservoir computing [8]. Previous

* Authors to whom any correspondence should be addressed.

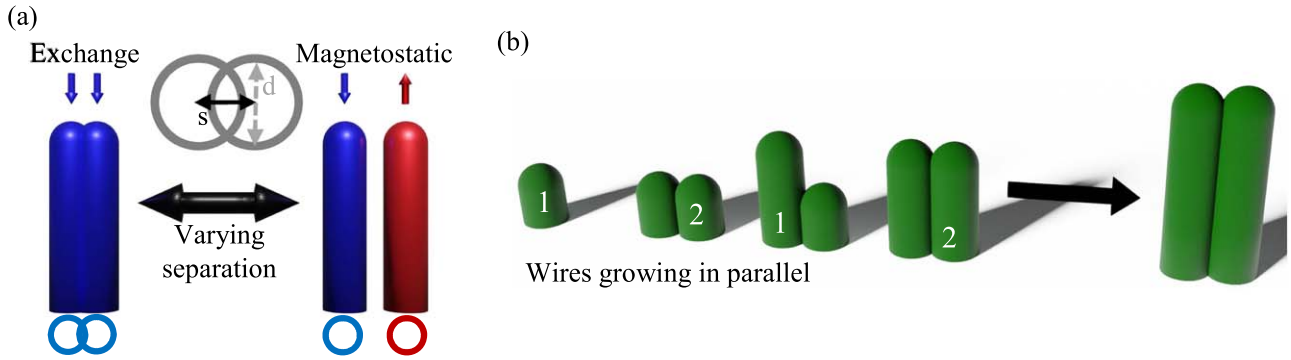

Figure 1. (a) Diagram showing how varying the separation of nanowires affects the magnetic interactions, with exchange interactions dominating for small separation and magnetostatic interactions dominating for large separations. The top inset shows that separation is defined as the distance between the centre of the two nanowires. Circles are shown below the wires to show how their cross-sections would appear. (b) Diagram showing parallel growth mechanism of nanowire pairs. Material is deposited sequentially between the nanowires until they reach the desired height.

research has mostly focused on rectangular nanostrips fabricated with thin film and planar lithography techniques [9–13]. Now, with new fabrication methods, it is possible to investigate three-dimensional (3D) magnetic systems [14–18]. In their simplest form, these are cylindrical nanowires, where new types of magnetic states can be supported. In particular, both the cylindrical symmetry and the aspect ratio have been shown to have a significant effect on the magnetic states of the system [19–22]. Typically, for isolated nanowires with small aspect ratios, the magnetisation will lie in the radial plane. With increasing height, this is followed by a vortex with an axial core and finally a uniform axial state. In this work we will refer to these states as 'Planar', 'Vortex' and 'Parallel', respectively. During fabrication, the aspect ratio will be constantly changing as the structure grows and therefore the magnetic state will continuously evolve through each of these states. Therefore, an important consideration is how a magnetic state may evolve during fabrication as this evolution can produce magnetic states that are distinct from the expected ground state.

Some of the fabrication techniques that allow this jump to 3D structures include: electrodeposition, two-photon lithography and focused electron beam induced deposition (FEBID). Utilising these techniques, the creation of more complex, 3D structures based on cylindrical nanowires can lead to the emergence of intricate domain structures [23–34]. One key area of interest for the development of spintronic devices is that of structures formed by strongly coupled nanowires [19, 35–43]. In the literature, this can be seen in the form of dense nanowire arrays, where promising spintronic properties may arise due to magnetostatic coupling; or if considering overlapped nanowires, exchange coupling is also introduced. In particular, FEBID has been shown to be an ideal nanofabrication technique for these investigations [31, 32, 35, 43]. For instance, strongly interacting helical nanowire pairs grown by FEBID can show locked pairs of domain walls in the case of separate wires and, when overlapped, chiral domain walls and topological 3D spin textures can form [35, 43]. However, these two previous works focused on helical nanowires, introducing a geometrically enforced chirality together with the magnetostatic and exchange energies. In this work, we focus instead on straight nanowires where geometric chirality does not play a role. Therefore, we can isolate the competition between exchange and magnetostatic energies in a coupled system. In these types of highly coupled structures, the magnetic state of one of the nanowires will have a large influence over the other, and vice versa, *from the very beginning of the fabrication process*. Here, through micromagnetic simulations, we investigate the evolution of magnetic states of highly coupled nanowire pairs grown in parallel as a function of interwire coupling and height. This procedure allows us to get an insight into how the magnetic states of the system varies with the strength of the inter-wire coupling, but also how a parallel growth strategy affects the final magnetic state of the system due to previously formed states.

2. Simulation setup and method

The micromagnetic simulation software Mumax3 [44] was used to mimic the growth of nanowires of varying separation. Cylindrical nanowire geometries with flat bottom and curved top caps were simulated to represent experimentally-fabricated wires. A small mesh size of 1.25 nm was chosen to more accurately represent a cylindrical geometry and to be below the characteristic exchange length of the material. The diameters of the nanowires were set to $d = 50$ nm and the centre-to-centre inter-wire distance, s, was varied from 0 (fully overlapped) to 60 nm (fully separated): see figure 1(a) for these details. By varying s [separation], we look to control the interaction between the exchange and magnetostatic energy (figure 1(a)). With lower s, we expect the system to tend towards an isolated nanowire, and hence towards a more exchange energy dominated system. Conversely with large s, we expect the magnetostatic energy to begin to dominate (see figure 2(c)). The Mumax3 in-built smoothing function was set to a value of 8 which, along with the small cell size, helped minimize staircase computational artefacts that can arise when simulating curved surfaces. We used micromagnetic

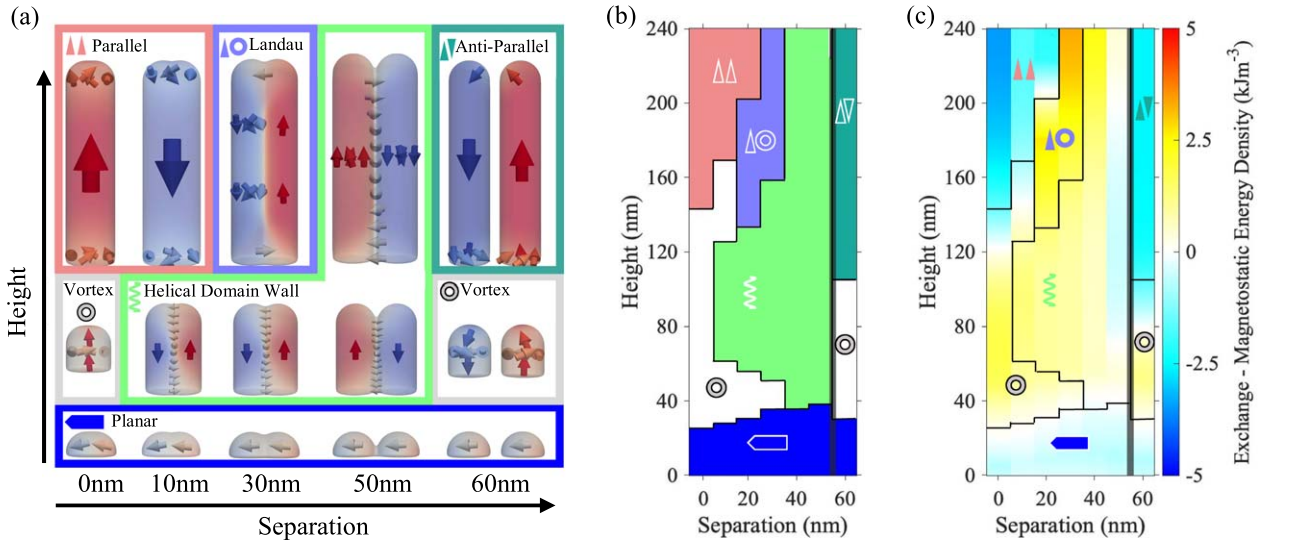

Figure 2. (a) A vector representation of the magnetic states that appear for varying separation and height. Each of the six states seen is given a colour and a symbol to match parts (b) and (c) of this figure as follows: planar—blue pentagon pointing right; vortex—grey donut; helical domain wall—green helix; parallel—pink upward triangles; Landau—purple triangle and donut; and anti-parallel—dark green opposite pointing triangles. (b) Phase diagram showing which of the 6 states are observed for each value of separation and height. Colours and symbols are defined in part a. The thick black vertical line at 55 nm separation marks where the nanowires are no longer overlapping. (c) Map of the difference between exchange and magnetostatic energies for each value of separation and height, in order to determine how the two energies compete. For example, regions where exchange energy dominates are red/yellow in tone. Overlaid symbols and black lines are to define which magnetic state is present at each point on the map. The thick black vertical line at 55 nm separation, marks where the nanowires are no longer overlapping.

parameters matching those typically obtained for FEBID cobalt [41]: saturation magnetisation, $M_s = 900 \times 10^3$ A m^{-1} (typically lower than the bulk); exchange stiffness, $A = 10^{-11}$ J m^{-1}, and zero magnetocrystalline anisotropy due to the nanocrystalline or amorphous nature of the material deposited in this manner [31, 43]. The geometry and material properties used here are also representative of common electrodeposited materials [41, 45–47]. Here, we simulate fully uniform structures, in terms of both material and geometry, as is expected for FEBID cobalt structures [35, 43]. Experimental variations, including chemical inhomogeneities, or shape dispersion are expected to be small and therefore only introduce random, local effects in the spin textures without altering the overall trends described here.

To study the evolution of the states during growth, sections of 5 nm in height were added to the top of each of the nanowires sequentially. This parallel method of growth is commonly used in FEBID [35, 43] (shown in figure 1(b)). The simulated structures were computationally grown to a height of 240 nm, as a compromise between simulating structures with an aspect ratio high enough to strongly favour axial magnetic configurations, and a reasonable computational time (simulations would typically take 1–5 h per growth step and were run on a NVIDIA GTX TITAN X graphical processing unit).

Each added section was given an initial random magnetic configuration. For all growth steps, the Landau–Lifshitz–Gilbert equation was integrated for the whole system (i.e. including the spins in both new and old sections) while the maximum torque of the system was $>10^{-4}$ T, with damping set at $\alpha = 0.5$. Once the above torque convergence criterion was reached, the magnetisation and energy densities were evaluated.

3. Results and discussion

3.1. Evolution of magnetic states in nanowire pairs

During the simulated fabrication of the nanowire pairs, we expect that the magnetic state that forms at each growth step depends strongly upon the geometry of the system, i.e. how tall the nanowires have been grown and the separation between them. Figure 2(a) shows a vector representation of the six main states obtained from simulations for the ranges of separation (0–60 nm) and height (0–240 nm) under investigation. Four of these states ('Planar', 'Vortex', 'Parallel' and 'anti-parallel') are as discussed the previous sections, appearing either for low heights or for extremes values of separation. The anti-parallel state occurs for separated nanowires where the uniform axial magnetic states form anti-parallel to each other due to magnetostatic coupling (top right of figure 1(a)). All simulations show the general trend of planar –> vortex-like –> axial, as the height of the wires increase. Two less conventional states are observed for intermediate degrees of overlap. We denote these the 'Landau pattern' and 'Helical domain-wall' states. These two magnetic configurations feature net anti-parallel wires, but with a complex emergent 3D domain structure. The classification of these 6 magnetic states is based on the observation of sharp changes in the energy profiles at the transitions between them (further discussed in section S1 of the supplementary documentation). These transitions are used in figure 2(b) to

generate a magnetic phase diagram as a function of height and separation. Figure 2(c) shows a map of the difference between exchange and magnetostatic energy density on the same axes, allowing the competition between energies to be evaluated for each state.

When the wires are fully overlapped (separation = 0 nm), they form a single cylindrical wire. During growth, the magnetic state evolves as previously reported in the literature for these geometries [19–22]: Planar—Vortex—Parallel (axial). Vortex caps of the same chirality are observed at the top and bottom of the Parallel state to reduce surface charges.

For the next simulation (separation = 10 nm), a new state appears—the 'Helical domain wall (DW) state'—evolving from the initial Planar and Vortex states (see figure 2(b)). This state is characterised by anti-parallel axial domains in the nanowires, with Néel caps at both ends and a DW in between them. In the bulk of the structure, a Bloch-type DW is favoured over a Néel-type DW to reduce magnetic volume charges. As the Néel caps at both ends are antiparallel to each other, the spins forming the wall spiral continuously for 180° around the z-axis with height, forming a helix (a vector profile is shown in the examples of the helical DW state figure 2(a)). The name 'Helical DW' is chosen from the profile of the spins in the region of overlap between the wires (this DW profile is reminiscent of both the 'Twisted DW' and 'Hybrid chiral DW' seen in [43] and [44] respectively). For this nanowire separation, and as the height increases during growth, the shape anisotropy of the long wire axis becomes increasingly dominant so that one of the axial domains is pushed out in favour of a Vortex state, finally followed by the Parallel state. For the next value of separation (20 nm), the growth will begin in a similar fashion. However, now the system transitions from a Helical DW state to the Parallel state, not through a Vortex, but instead via what we denominate a 3D 'Landau pattern' (named due to its resemblance to a Landau–Lifshitz pattern [48]). This state is similar to that previously described for rectangular magnetic systems, and consists of two anti-parallel domains [49, 50]. Here, however, the magnetisation in one wire is strongly axial (red, net $+M_z$ domain in figure 2(a)), and takes the form of a vortex in the other (blue, net $-M_z$ domain). Due to their complex nature, both the Landau pattern and Helical DW states will be discussed in more detail in section 3.2.

For the subsequent simulations with larger separation between the wires, the final state of the structure (up to the full height that was simulated) consists of anti-parallel domains. The domain structure is defined by the thickness of the region of overlap between the wires. At a separation of 30 nm, the Landau pattern state is the final state achieved. For the next two values of separation (40 and 50 nm, figure 2(b)), the final state is the Helical DW. It can also be noted that at these separations, the Planar state transitions directly into the Helical DW state without going through a Vortex, due to the larger separation favouring anti-parallel magnetostatic coupling between the wires.

Finally, when the wires are fully separated (60 nm), the two individual wires follow a similar growth pattern to the fully overlapped simulations (separation of 0 nm, an isolated nanowire). However, for separated wires, the inter-wire magnetostatic coupling means that the vortex cores in each wire form anti-parallel to each other. Additionally, the formation of single domain axial states also occurs at lower heights than for the single wire, and the caps at the tops of the wires become reminiscent of Néel caps (due in part to their rounded geometry).

Figure 2(c) shows the difference between the exchange and magnetostatic energy densities, in order to evaluate which one dominates for each geometry. As expected, for colinear states (Planar or Parallel) the exchange energy is lower than the magnetostatic energy. Conversely, more complex magnetic states (Vortex, Helical DW, Landau pattern) correspond to a higher exchange energy density, due to the formation of non-collinear spin configurations. Out of all the states found in the simulations, the Landau pattern is the most costly in exchange energy density, followed by the Helical DW and Vortex states, which have similar values. These results show that for the design of coupled geometries capable of stabilising complex spin textures, care must be taken to ensure that the coupling between the structures has an appropriate intermediate value to allow the magnetic energies to compete with each other (i.e. not allowing one to dominate over the other). In the case of this study, this is observed when the overlapped wires form a net magnetic anti-parallel alignment to each other.

3.2. Emerging three dimensional magnetic states for intermediate overlapping

For intermediate separation, the coupled nanowire system tends to evolve towards states where the magnetostatic energy is minimized by aligning the overall magnetisation of both wires anti-parallel to each other. However, in doing so, an increase in exchange energy takes place due to the formation of complex 3D domain structures. The type of configuration that forms is defined by the thickness of the overlapping region between the wires. A comparison between the two states emerging for intermediate overlapping is shown in figure 3 with views along each axis. The viewing directions for figures 3(d)–(f) are shown in 3a-c respectively. Figure 3(d) shows a side view for both states on the left and right: a colour plot of the M_x component on a slice in the overlapping region of the wires and an isosurface of spins within 10% of the $-M_y$ component to visualise the domain wall. The top central inset of figure 3(d) corresponds to the M_x component as a function of height along the z-axis for the middle overlapping area, as marked by coloured dashed lines overlaid on the simulation plots. The bottom inset shows a detailed zoom-in of the magnetic configuration for the Landau pattern where the DW meets the surface. Figures 3(e) and (f) complement figure 3(d) by plotting a front view of the M_z isosurfaces (figure 3(e)) and xy projections of the magnetisation vector coloured by M_z (figure 3(f)) for seven representative heights along the z axis (locations of which are marked with grey dashed lines in figure 3(e)).

We first focus on the Landau pattern state. In this case, the overlapping region is nearly as thick as the wires

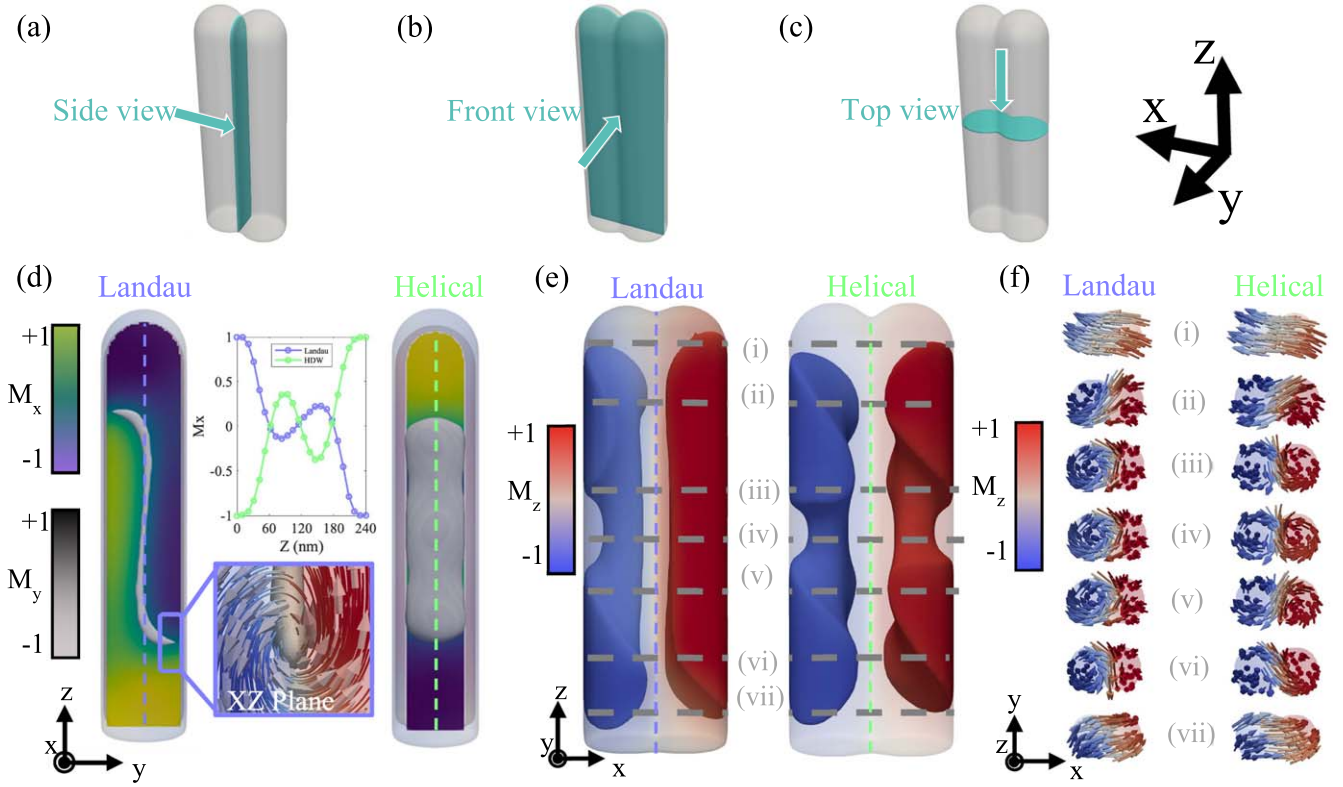

Figure 3. (a), (b), (c) Viewpoints for figures (d), (e) and (f) respectively. (d) Left and right sections show a side view of the Landau pattern and helical DW state respectively, coloured by the M_x-component in a central slice. A 2% isosurface in each of spins within 2% of the negative y-axis (grey surface) is shown to highlight the different domain structures between the simulations. The top central inset shows a plot of the M_x component versus Z-coordinate in the centre of the structure (purple and green dotted lines respectively) to highlight the modulation seen in the profile of the domain wall. The bottom inset shows a vortex in the XZ plane around the location where the Landau domain meets the surface of the structure. (e) Left and right sections show a front view of 10% $+/-$ M_z isosurfaces of the Landau pattern and helical DW state, respectively, to highlight the differences in the anti-parallel domains of both states. The Landau pattern shows a vortex-axial configuration while the helical DW shows a double vortex state. Coloured dotted lines show the location of the spins plotted in the top inset of part d and grey dotted lines are the locations of the cross-sections shown in (f). (f) Left and right sections show XY cross-sections of the Landau pattern and helical DW state respectively, coloured by the M_z component at the locations of the grey dotted lines in part (e). These are to show the differences in the anti-parallel domain structure between the two states, and also the transition between the caps and the bulk of the structures.

themselves (in the y-direction, shown in figure 3(d)), and thus allows for the extension of the Néel caps along the surface of the structure (shown as yellow on the left and purple on the right in figure 3(d)). This magnetic state reduces surface charges and creates an S-shaped DW (grey isosurfaces in figure 3(d)) between the wires that only has one point on each of its edges where it meets the surface of the structure (see left panel in figure 3(d) and the corresponding bottom inset) [49, 50]. A notable feature of this magnetic state is that the anti-parallel domains are not equivalent: whereas in one wire (the net $+M_z$ domain, red in figure 3(e)) the magnetisation is strongly aligned with the z-axis, the domain in the other wire (the net $-M_z$ domain, blue in figure 3(e)) takes the form of a vortex. In fact, this structure contains one single vortex tube that begins and ends at the two points where the Landau domain meets the surface of the structure. However, the vortex does not follow the Landau domain within the bulk of the structure (in-between cross-sections iii and iv in figure 3(e)). Instead, it extends through the net $-M_z$ domain, resulting in a vortex extending along the length of this wire (distinguishing this state from a Landau–Lifshitz pattern in a rectangular geometry [50]). This is due to the vortex being able to adapt easily to the cylindrical geometry of one of the wires. Cross-section iv of the Landau pattern in figure 3(f) highlights this vortex-axial configuration in the net structure of anti-parallel domains. The other cross-sections in this figure show the transition between the ends, where Néel caps are formed at top and bottom, and the body of the structure, where the magnetisation evolves towards a vortex-axial configuration.

The second emergent 3D magnetic state observed in the simulations for intermediate overlap is the Helical DW. In comparison with the Landau pattern, the two anti-parallel domains of the wires in any Helical DW state are equivalent to each other. When the state first forms, the anti-parallel domains are strongly axial. However, with increasing height, they both become more vortex-like (with opposite cores and circulations, and hence, the same chirality). Cross-section iv (for the Helical DW) in figure 3(f) shows this double vortex configuration of the domains in the mid-point of the structure.

For the Helical DW, the region in-between the wires is typically smaller than in the previous case discussed

($s = 30$ nm), inhibiting the formation of a Landau pattern due to the high cost in exchange energy. Instead, a Bloch-like DW is formed between the wires. As mentioned in section 3.1, the DW observed here bears resemblance to DWs reported in [48, 51, 52]. For low heights, the Helical DW displays the same continuous rotation of spins (when going from the bottom to the top of the structure) as reported in those references. However, with further growth, our Helical DW develops a sinusoidal modulation (as seen when plotting the M_x component across the Néel caps and DW, top inset in figure 3(d)). We understand that the modulation forms to oppose the charges created by the Néel caps (and is therefore bound to it). The formation of the modulation in the Helical DW is strongly dependant on the volume magnetic charges. Figure 4 plots the divergence of magnetisation as a way to visualise the magnetic charges in the system. Figure 4(a) shows how the charge distribution evolves during the simulation with $s = 40$ nm (for a front view of the magnetisation). For a vortex state, positive and negative magnetic charges appear at the top and bottom of the structure, respectively. When the Helical DW state forms however, we see 8 alternating regions of positive and negative magnetic charges arrange themselves in a swirl-like pattern to reduce magnetostatic energy. This pattern is very reminiscent of the swirls and helical patterns of magnetisation discussed in [53]. As the structure continues to grow, we see a region of zero divergence split the top four and bottom four areas of alternating charge, creating a pure Bloch DW in-between the anti-parallel domains.

Figure 4(b) shows a comparison between two final magnetic states ($s = 30$ nm for the Landau pattern and $s = 40$ nm for the Helical DW state). On the right hand side, we have a fully grown Helical DW, which shows 4 regions of magnetic charge appearing in the body of the structure (in addition to the 8 charges at the Néel caps). It is these areas of charge that lead to the appearance of the modulation in the DW (top inset in figure 3(d)). They are formed to reduce magnetostatic energy and oppose the 4 regions of charge that are confined in both Néel caps. We have thus regions of pure Bloch character appearing, where the divergence drops to zero, and deviations from a pure Bloch DW where the magnetic charges appear (how the Helical DW evolves with continued growth is discussed in the section S2 of the supplementary information). In the top and side view (orange and blue boxes to the right hand side of figure 4(b)), we see large regions of positive and negative magnetic charge on the outside of the indent between the wires. The left hand side of figure 4(b) shows the same representations for a fully grown Landau pattern state. In the front view, a similar magnetic charge distribution to what is seen in the Helical DW is observed. The main difference is that the regions of charge in the body of the structure are stronger in the left wire. This is because the net M_z domain on the right hand side is very strongly axial and so has a lower divergence. In the top view to the left (left orange box), we see four regions of alternating magnetic charge that are not centred around the vortex in the net axial domain of the left wire, but are instead centred around the indent between the wires. In the side view of figure 4(b) (left blue box), we see the strongest regions of charge appearing where the Landau domain meets the surface of the structure (with regions of opposite magnetic charge in the centre to offset those).

The emergence of both the Helical DW and the Landau pattern show the influence that competing magnetic coupling between wires can have on the magnetic states available to the system. We also demonstrate how the exchange and magnetostatic energies can compete in more subtle ways and how this can influence the structure of a DW. However, as discussed in the introduction, we also want to investigate the effect of the growth history of the system. Therefore, in the next section we examine the impact of the parallel growth mechanism on the states formed.

3.3. Induction of metastable states via the parallel growth method

Given that we are simulating a parallel growth mechanism, (i.e. two wires growing at the same time in small sequential steps) the equilibrium magnetic state reached may not necessarily be the ground state. To investigate the effect of the growth mechanism, the regions of stability for each of the fully grown overlapped states (i.e. Parallel, Landau pattern and Helical DW) were investigated between separations of 10 and 50 nm (as these were the values of separation that marked out the limits of structures consisting of two overlapped nanowires). The output of a growth simulation was selected for each state: $s = 10$ nm for Parallel, 30 nm for Landau pattern and 50 nm for Helical DW. The separation of the wires was then increased or reduced by one cell at a time. Any new cells introduced were given a random magnetisation. At this new value of separation, the system was allowed to evolve dynamically to ascertain if the state in question would be stable (to the same criterion as the growth simulations described in section 2). If the state remained stable, the energy was evaluated and the separation was altered by one cell again. This process was repeated until either the state was no longer stable or the full range of separation had been probed.

Figure 5 shows the energy of each of these states at every value of separation where they remained stable. From this protocol, it is observed that the Parallel state remains metastable for all degrees of overlap, despite not forming during our simulated growth procedure for separation $\geqslant$30 nm. The energy density of the Parallel state increases with separation due to magnetostatic energy becoming more costly (this relationship varies from a linear trend for separations above 45 nm, due to subtle changes in the magnetic configuration of the caps of the structure). The Helical DW state however, shows the opposite trend, with energy density increasing with decreasing separation until it collapses into the Landau pattern below separations of 31.25 nm. The trends for these two states show the expected trade-off between the magnetostatic and exchange energies, with a cross-over in ground state as magnetostatic energy dominates at higher separations and exchange dominates at lower separations (figure 1(a)). The Landau pattern shows a similar energy trend to that of the Helical DW, and is stable between separations of 22.5 and

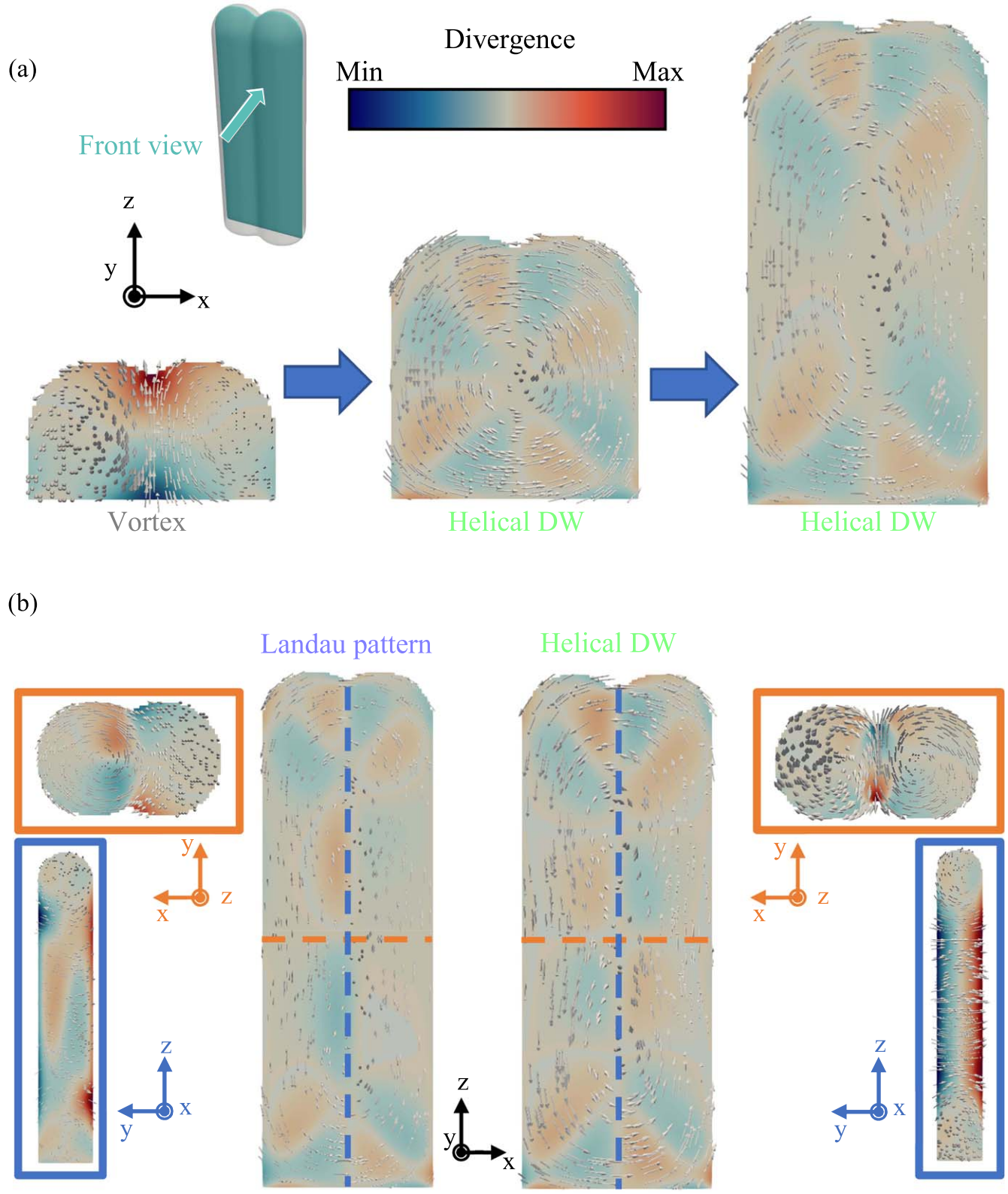

Figure 4. (a) A front view during growth of simulation of nanowire pairs of 30 nm separation, coloured by the divergence of magnetisation to show magnetic charges. Magnetic vectors are overlaid to show the direction of magnetisation, but are not coloured. As the wires grow, the magnetic state changes from vortex to helical domain wall. (b) Comparison of magnetic charges for two 'fully grown' magnetic states: left—Landau pattern, 15 nm separation; right—Helical DW, 20 nm separation. For each a front view is shown as in part (a). Blue and orange dashed lines show locations of side and top views, respectively, that are plotted on the sides of the figure.

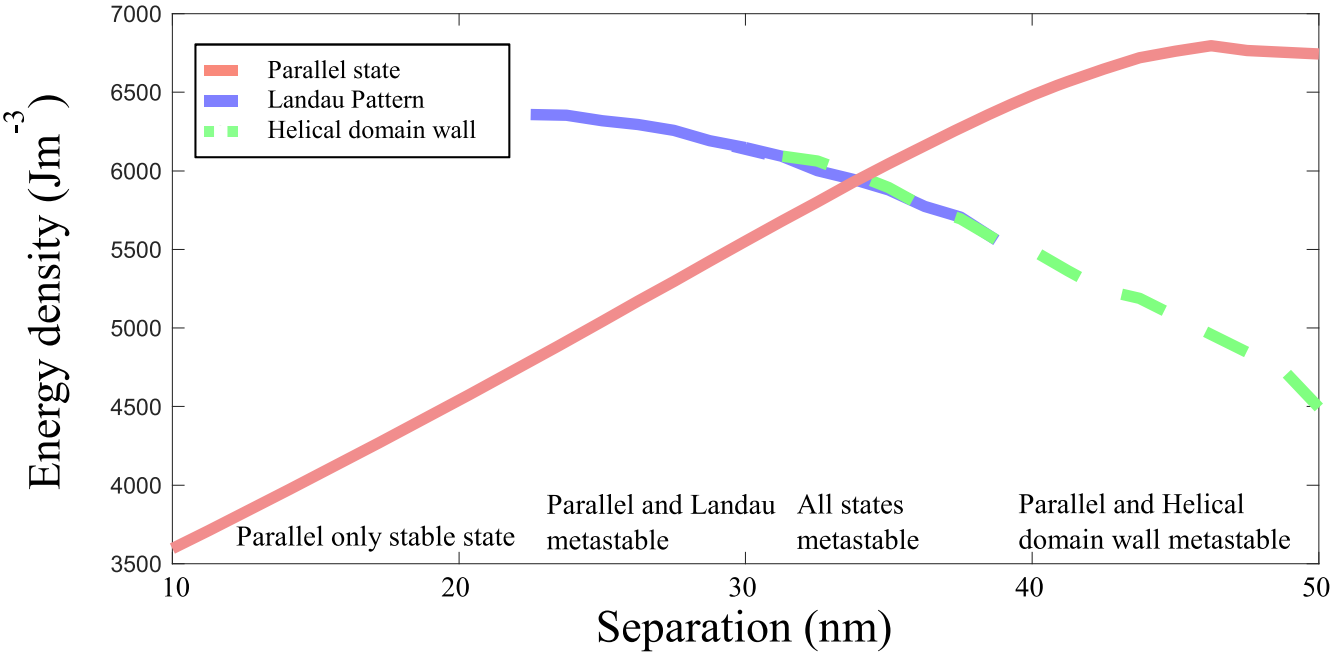

Figure 5. Relative energies of metastable states in fully grown (240 nm) nanowire pairs for different interwire separation; Parallel—red, Landau pattern—purple and Helical DW—green. The energy profile of the Helical DW is shown using a dashed line so that both remain visible when they overlap The energy of each magnetic state was evaluated for each value of separation where it was observed to be stable. The regions of stability of the Landau pattern (intermediate separation values) and Helical DW (largest separation values) are marked out with vertical dotted lines of their corresponding colour. The parallel state is always stable for all values of separation.

38.75 nm. Below 22.5 nm, the Parallel state is the only stable configuration of the system, and above 38.75 nm the overlapping region between the wires becomes too small and prevents the Landau pattern from forming (as discussed in section 3.2).

As shown in figure 5, there are three regions where multiple states coexist. Above 38.75 nm the Parallel and Helical DW states can form. However, the saving in magnetostatic energy from having an anti-parallel alignment between the wires means that the Helical DW is the ground state. This fact lines up with the growth simulations, as the Helical DW was achieved as the final state for separations of 40 and 50 nm. Between 31.35 and 38.75 nm, all three states are metastable with each other. The energy densities of the Landau pattern and Helical DW have very similar values in this region as their respective savings of magnetostatic and exchange energy over each other effectively cancel out in this region. The ground state switches in this region from an anti-parallel alignment of wires to a parallel one below 34 nm, which remains the case for any nanowire pair with a smaller value of separation.

The most revealing aspect of this method of simulation is highlighted in the final region of metastability. Between 22.5 and 31.25 nm only the Landau pattern and the parallel state can exist, but the most energetically favourable state is the parallel state, due to its savings in exchange energy. Nevertheless, for separations of 30 nm, it is the Landau pattern that forms during our growth simulations. In the parallel growth mechanism utilised here, the small aspect ratio seen at the start of growth favours an anti-parallel alignment between the wires. As the aspect ratio increases, the parallel state will become more energetically favourable [15–18]. However, an energy barrier may form, preventing the annihilation of one of the domains. For lower separations, this energy barrier can be overcome (e.g. for a separation of 20 nm, figure 2(b)). Conversely, for a separation of 30 nm, the energy barrier is high enough to prevent this transition. A common method to explore the magnetic state of a nanowire involves relaxing the system from a saturated state [48, 49]. In this case however, due to the metastability of the Parallel state at all separations, this method would not return the overlapped anti-parallel states presented here. Consequently, we would be building an inaccurate picture of the effect of the magnetic coupling. Contrastingly, the controlled-evolution method used here gives a more comprehensive depiction of this type of system.

The results presented here highlight the influence and control that the fabrication method can exert on the magnetic state of the system. In particular, a direct-write technique such as FEBID allows for significantly different growth strategies to be employed to realize the same geometry (e.g. fully growing one wire before starting on the second may produce a different as-grown magnetic remanent state).

4. Conclusion

We have presented a simulation study of the control of magnetic states through both the tuning of coupling between nanowire pairs and parallel fabrication of the nanowires. Together, this leads to the formation of a wide variety of 3D magnetic states. Included in these are the Landau pattern and modulated helical DW, which both only form for limited

combinations of height and separation. We show the influence of magnetic volume charges on the DW structure by revealing a modulated DW with a mixture of Bloch and Néel character. The impact that the fabrication process can have on the magnetic state of the system is revealed. The parallel-growth method followed here favours an anti-parallel magnetic coupling between the wires, even when not the ground state, which leads to complex 3D domain structures forming between the two opposite domains in both wires. This result exemplifies the influence that the fabrication method has over the magnetic configuration of a given system.

The growth simulation method presented here could be expanded to mimic different fabrication techniques (e.g. electrodeposition, electroless deposition and atomic layer deposition) [52, 53]. It would also allow for the addition of further complexities. For example, a radial growth process could be employed in the place of, or together with, the axial process shown here [54, 55]. Magnetocrystalline or magnetoelastic anisotropies could be introduced, thereby adding a third magnetic energy to the competition [52]. Furthermore, we could consider variations of composition and geometry along the length of the wire [24, 25, 56–62]. The understanding how different degrees of magnetic coupling may affect magnetic states in nanostructures is important for many sub-areas of nanomagnetism, from biomagnetism to spintronics, and will assist in the understanding and design of coupled 3D nanostructures.

Acknowledgments

The authors would like to thank Naemi Leo and Jakub Jurckyck from CSIC in Zaragoza and Miguel A Cascales Sandoval from the University of Glasgow for fruitful discussions. We would also like to thank Sam McFadzean at the Kelvin Nanofabrication centre in Glasgow for technical support, and the University of Glasgow where this work was carried out. This work was supported by the EPSRC and the Centre for Doctoral Training (CDT) in Photonic Integration and Advanced Data Storage (PIADS), RCUK Grant No. EP/L015323/1, the European Community under the Horizon 2020 Program, Contract No. 101001290 (3DNANOMAG), the MCIN with funding from European Union NextGenerationEU (PRTR-C17.I1), and the Aragon Government through the Project Q-MAD. AH-R acknowledges the support from European Union's Horizon 2020 research and innovation program under Marie Skłodowska-Curie Grant ref. H2020-MSCA-IF-2016-746958, from the Spanish MICIN under Grant PID2019-104604RB/AEI/10.13039/501100011033 and from the Asturias FICYT under Grant AYUD/2021/51185 with the support of FEDER funds. *CINN (CSIC—Universidad de Oviedo), El Entrego, Spain* LS acknowledges support from the University of Cambridge (EPSRC Cambridge NanoDTC EP/L015978/1) DH acknowledges Unité Mixte de Physique, CNRS, Thales, Université Paris-Saclay, 91767, Palaiseau, France. CD acknowledges funding from the Max Planck Society Lise Meitner Excellence Program.

Data availability statement

All data that support the findings of this study are included within the article (and any supplementary files).

ORCID iDs

J Fullerton https://orcid.org/0000-0002-7527-7034
A Hierro-Rodriguez https://orcid.org/0000-0001-6600-7801

References

[1] Parkin S S P, Hayashi M and Thomas L 2008 Magnetic domain-wall racetrack memory *Science* **320** 190
[2] Rial J and Proenca M P 2020 A novel design of a 3D racetrack memory device based on functional segments in cylindrical nanowire arrays *Nanomaterials* **10** 2403
[3] Allwood D A, Xiong G, Faulkner C C, Atkinson D, Petit D and Cowburn R P 2005 Magnetic domain-wall logic *Science* **309** 5741
[4] Ivanov Y P, Alfadhel A, Alnassar M, Perez J E, Vazquez M, Chuvilin and Kosel J 2016 Tunable magnetic nanowires for biomedical and harsh environment applications *Sci. Rep.* **6** 24189
[5] Martínez-Banderas A I *et al* 2019 Iron-based core–shell nanowires for combinatorial drug delivery and photothermal and magnetic therapy *ASC. Appl. Matter. Interfaces* **11** 43976
[6] Pondman K M, Bunt N D, Maijenburg A W, van Wezel R J A, Kishore U, Abelmann L, ten Elshof J E and ten Haken B 2015 Magnetic drug delivery with FePd nanowires *J. Magn. Magn. Mater.* **380** 299
[7] Yan S H, Ryu K S and Parkin S 2015 Domain-wall velocities of up to 750 ms^{-1} driven by exchange-coupling torque in synthetic antiferromagnets *Nat. Nanotech.* **10** 221
[8] Dawidek R W *et al* 2021 Dynamically driven emergence in a nanomagnetic system *Adv. Funct. Mater.* **31** 2008389
[9] Atkinson D, Eastwood D S and Bogart L K 2008 Controlling domain wall pinning in planar nanowires by selecting domain wall type and its application in a memory concept *Appl. Phys. Lett.* **92** 022510
[10] Bogart L K, Atkinson D, O'Shea K, McGrouther D and McVitie S 2009 Dependence of domain wall pinning potential landscapes on domain wall chirality and pinning site geometry in planar nanowires *Phys. Rev.* B **79** 054414
[11] Lewis E R, Petit D, Jausovec A-V, O'Brien L, Read D E, Zeng H T and Cowburn R P 2009 Measuring domain wall fidelity lengths using a chirality filter *Phys. Rev. Lett.* **102** 057209
[12] Brandão J, Novak R L, Lozano H, Soledade P R, Mello A, Garcia F and Sampaio L C 2014 Control of the magnetic vortex chirality in permalloy nanowires with asymmetric notches *J. Appl. Phys.* **116** 193902
[13] Brandão J and Atkinson D 2016 Controlling the stablility of both the structure and velocity of domain walls in magnetic nanowires *Appl. Phys. Lett.* **109** 062405
[14] Fernández-Pacheco A, Streubel R, Fruchart O, Hertel R, Fischer P and Cowburn R P 2017 Three-dimensional nanomagnetism *Nat. Commun.* **8** 15756
[15] Gu K, Guan Y, Hazra B K, Deniz H, Migliorini A, Zhang W and Parkin S S P 2022 Three-dimensional racetrack memory devices designed from freestanding magnetic heterostructures *Nat. Nanotechnol.* **17** 1065

[16] Puydinger dos Santos M V, Brandão J, Dugato D A, Béron F, Pirota K R and Utke I 2020 Annealed cobalt-carbon nanocomposites for room-temperature spintronic applications *ASC. Nano. Mater.* **3** 7143

[17] Meng F *et al* 2021 Non-planar geometrical effects on the magnetoelectrical signal in a three-dimensional nanomagnetic circuit *ASC. Nano. Mater.* **15** 6765

[18] Weitzer A, Huth M, Kothleitner G and Plank H 2022 Expanding FEBID-based 3D-nanoprinting towards closed high-fidelity nanoarchitectures *ASC. Appl. Electron. Mater.* **4** 744

[19] Ross C A *et al* 2002 Micromagnetic behaviour of electrodeposited cylinder arrays *Phys. Rev.* **65** 144417

[20] Porrati F and Huth M 2004 Diagram of the states in arrays of iron nanocylinders *Appl. Phys. Lett.* **85** 3157

[21] Metlov K L and Lee Y 2008 Map of metastable states for thin circular magnetic nanocylinders *Appl. Phys. Lett.* **91** 112506

[22] Guslienko K Y, Choe S B and Shin S C 2000 Reorientational magnetic transition in high-density arrays of single-domain dots *Appl. Phys. Lett.* **85** 3609

[23] Ivanov Y P, Trabada D G, Chuvilin A, Kosel J, Chubykalo-Fesenko O and Vázquez M 2014 Crystallographically driven magnetic behaviour of arrays of monocrystalline Co nanowires *Nanotechnology* **25** 475702

[24] Ruiz-Gómez S, Foerster M, Aballe L, Proenca M P, Lucas I, Prieto J L, Mascaraque A, de la Figuera J, Quesada A and Pérez L 2018 Observation of a topologically protected state in a magnetic domain wall stabilized by a ferromagnetic chemical barrier *Sci. Rep.* **8** 16695

[25] Bran C *et al* 2020 Unveiling the origin of multidomain structures in compositionally modulated cylindrical magnetic nanowires *ASC. Nano* **14** 12819

[26] Wagner M F P, Paulus A S, Brötz J, Sigle W, Trautmann C, Voss K-O, Völklein F and Toimil-Molares M E 2021 Effects of size reduction on the electrical transport properties of 3D Bi nanowire networks *Adv. Electron. Mater.* **7** 2001069

[27] Li J, Sattayasamitsathit S, Dong R, Gao W, Tam R, Feng X, Ai S and Wang J 2014 Template electrosynthesis of tailored-made helical swimmers *Nanoscale* **6** 9415

[28] Askey J, Hunt M O, Langbein W and Ladak S 2020 Use of two-photon lithography with a negative resist and processing to realise cylindrical magnetic nanowires *Nanomaterials* **10** 429

[29] Williams G *et al* 2017 Two-photon lithography for 3D magnetic nanostructure fabrication *Nano Res.* **11** 845

[30] Martín J I, Vélez M, Morales R, Alameda J M, Anguita J V, Briones F and Vicent J L 2002 Fabrication and magnetic properties of arrays of amorphous and polycrystalline ferromagnetic nanowires obtained by electron beam lithography *J. Magn. Magn. Matter.* **249** 156

[31] Pablo-Navarro J, Magén C and de Teresa J M 2018 Purified and crystalline three-dimensional electron-beam-induced-deposits: the successful case of cobalt for high-performance magnetic nanowires *ASC Appl. Nanomater.* **1** 38

[32] Skoric L, Sanz-Hernández D, Meng F, Donnelly C, Merino-Aceituno S and Fernández-Pacheco A 2020 Layer-by-layer growth of complex shaped three-dimensional nanostructures with focused electron beams *Nano Lett.* **20** 184

[33] Gavagnin M, Wanzenboeck H D, Wachter S, Shawrav M M, Persson A, Gunnarsson K, Svedlindh P, Stöger-Pollach M and Bertagnolli E 2014 Free-standing magnetic nanopillars for 3D nanomagnet logic *ASC Appl. Mater. Interfaces* **6** 20254

[34] Sanz-Hernández D *et al* 2018 Fabrication of scaffold-based 3D magnetic nanowires for domain wall applications *Nanomatter* **8** 483

[35] Donnelly C *et al* 2022 Complex free-space magnetic field textures induced by three-dimensional magnetic nanostructures *Nat. Nanotechnol.* **17** 136

[36] May A, Hunt M, van den Berg A, Hejazi A and Ladak S 2019 Realisation of a frustrated 3D magnetic nanowire lattice *Commun. Phys.* **2** 13

[37] da Câmara Santa Clara Gomes T, Marchal N, Abreu Araujo F, Galván Y V, de la Torre Medina J and Piraux L 2021 Magneto-transport in flexible 3D networks made of interconnected magnetic nanowires and nanotubes *Nanomatter* **11** 221

[38] Burks E C, Gilbert D A, Murray P D, Flores C, Felter T E, Charnvanichborikarn S, Kucheyev S O, Colvin J D, YinG and Liu K 2021 3D nanomagnetism in low density interconnected nanowire networks *Nano Lett.* **21** 716

[39] Ojha S, Nunes W C, Aimon N M and Ross C A 2016 Magnetostatic interactions in self-assembled $Co_xNi_{1-x}Fe_2O_4/BiFeO_3$ multiferroic nanocomposites *ASC Nano* **10** 7657

[40] Dmytriiev O *et al* 2013 Static and dynamic magnetic properties of densely packed magnetic nanowire arrays *Phys. Rev.* B **87** 174429

[41] Shima M, Hwang M and Ross C A 2002 Magnetic behavior of amorphous CoP cylinder arrays *J. Appl. Phys.* **93** 3441

[42] Grutter A J, Krycka K L, Tartakovskaya E V, Borchers J A, Reddy K S M, Ortega E, Ponce A and Stadler B J H 2017 Complex three-dimensional magnetic ordering in segmented nanowire arrays *ASC Nano* **11** 8311

[43] Sanz-Hernández D *et al* 2020 Artificial double-helix for geometrical control of magnetic chirality *ASC Nano* **14** 8084

[44] Vansteenkiste A, Leliaert J, Dvornik M, Helsen M, Garcia-Sanchez F and van Waeyenberge B 2014 The design and verification of MuMax3 *AIP Adv.* **4** 107133

[45] Bukharia K, Karmakar P, Pandit P and Gupta A 2021 Study of magnetic nanowires of amorphous $Co_{20}Fe_{60}B_{20}$ prepared by oblique angle deposition on nanorippled substrate *J. Magn. Magn. Matter.* **529** 167842

[46] Chiriac H, Moga A, Urse M, Paduraru I and Lupu N 2003 Preparation and magnetic properties of amorphous NiP and CoP nanowire arrays *Jour. Magn. Magn. Matter.* **272** 1678

[47] Cui C, Chen F, Yang W, Li H, Liu Q and Sun J 2015 Electrochemical fabrication, microstructure and magnetic properties of Sm_2Co_{17}/Fe_7Co_3 dual phase nanocomposite *Mater. Chem. Phys.* **160** 315

[48] Legrand W, Chauleau J-Y, Maccariello D, Reyren N, Collin S, Bouzehouane K, Jaouen N, Cros V and Fert A 2018 Hybrid chiral domain walls and skyrmions in magnetic multilayers *Sci. Adv.* **4** 0415

[49] Arrott A S and Templeton T L 2017 Using magnetic charge to understand soft-magnetic materials *AIP Adv.* **8** 047301

[50] Nguyen V D, Fruchart O, Pizzini S, Vogel J, Toussaint J-C and Rougemaille N 2015 Third type of domain wall in soft magnetic nanostrips *Sci. Rep.* **5** 12417

[51] Lemesh I and Beach G S D 2018 Twisted domain walls and skyrmions in perpendicularly magnetized multilayers *Phys. Rev.* B **98** 104402

[52] Fallon K, McVitie S, Legrand W, Ajejas F, Maccariello D, Collin S, Cros V and Reyren N 2019 Quantitative imaging of hybrid chiral spin textures in magnetic multilayer systems by Lorentz microscopy *Phys. Rev.*B **100** 214431

[53] Templeton T L, Hanham S D and Arrott A S 2018 Helical patterns of magnetization and magnetic charge density in iron whiskers *AIP Adv.* **8** 056022

[54] Ruffer D *et al* 2014 Anisotropic magnetoresistance of individual CoFeB and Ni nanotubes with values of up to 1.4% at room temperature *APL Mater.* **2** 076112

[55] Rohan J F, Casey D P, Ahern B M, Rhen F M F, Roy S, Fleming D and Lawrence S E 2008 Coaxial metal and magnetic alloy nanotubes in polycarbonate templates by electroless deposition *Electrochem. Commun.* **10** 1419

[56] Chong Y T, Görlitz D, Martens S, Yau M Y E, Allende S, Bachmann J and Nielsch K 2010 Multilayered core/shell nanowires displaying two distinct magnetic switching events *Adv. Mater.* **22** 2435

[57] Fernández-González C *et al* 2022 Electrodeposited magnetic nanowires with radial modulation of composition *Nanomaterial* **12** 2565

[58] Bran C, Fernandez-Roldan J A, del Real R P, Asenjo A, Chubykalo-Fesenko O and Vazquez M 2021 Magnetic configuration in modulated cylindrical nanowires *Nanomaterial* **11** 600

[59] Fernandez-Roldan J A, de Riz A, Trapp B, Thirion C, Vazquez M, Toussaint J-C, Fruchart O and Gusakova D 2019 Modelling magnetic-field-induced domain wall propagation in modulated-diameter cylindrical nanowires *Sci. Rep.* **9** 5130

[60] Berganza E, Jaafar M, Bran C, Fernandez-Roldan J A, Chubykalo-Fesenko O, Vazquez M and Asenjo A 2017 Multisegmented nanowires: a step towards the control of the domain wall configuration *Sci. Rep.* **7** 11576

[61] Rodriguez L A, Bran C, Reyes D, Berganza E, Vazquez M, Gatel C, Snoeck E and Asenjo A 2016 Quantitative nanoscale magnetic study of isolated diameter-modulated FeCoCu nanowires *ACS Nano* **10** 9669

[62] Andersen I M *et al* 2021 Field tunable three-dimensional magnetic nanotextures in cobalt-nickel nanowires *Phys. Rev. Res.* **3** 033085